AUGUST 01 2000

Experimental study of sound propagation in a flexible duct

Lixi Huang; Y. S. Choy; R. M. C. So; T. L. Chong

J. Acoust. Soc. Am. 108, 624–631 (2000)
https://doi.org/10.1121/1.429594

Experimental study of sound propagation in a flexible duct

Lixi Huang, Y. S. Choy, R. M. C. So, and T. L. Chong
Department of Mechanical Engineering, The Hong Kong Polytechnic University, Kowloon, Hong Kong

(Received 8 June 1999; accepted for publication 5 May 2000)

Propagation of sound in a flexible duct is investigated both theoretically and experimentally. Strong coupling of sound and flexural waves on the duct wall is found when the wall-to-air mass ratio is of the order of unity. The axial phase speed of sound approaches the *in vacuo* speed of flexural waves (subsonic in this case) at low frequencies. However, a speed higher than the isentropic sound speed in free space (340 m/s) is found beyond a critical frequency which is a function of the mass ratio. Experiments using a duct with a finite section of tensioned membrane are compared with the propagating modes pertaining to the infinite membrane model. Satisfactory quantitative agreement is obtained and the measured phase speed ranges from 8.3 to 1348 m/s. In the moderate frequency range, the theory predicts high spatial damping rate for the subsonic waves, which is consistent with the experimental observation that subsonic waves become increasingly undetectable as the frequency increases. Substantial sound reflection is observed at the interface between the rigid and the flexible segments of the duct without cross-section discontinuity, which, together with the high spatial damping, could form a basis for passive control of low-frequency duct noise. © *2000 Acoustical Society of America.* [S0001-4966(00)03308-7]

PACS numbers: 43.50.Gf, 43.20.Mv, 43.20.Hq [MRS]

INTRODUCTION

Strong sound–structure coupling normally occurs in underwater applications where the fluid density is of the same order of magnitude as the structural density (Fahy, 1997); the same in air is possible at the presence of substantial flow speed. This article reports strong air–structure coupling without flow in a chosen parameter range and the work is motivated by the prospect of devising smart structures for broadband passive control of low-frequency noise, which is hitherto more effectively dealt with by active noise control techniques. In traditional passive noise control (Beranek and Ver, 1992), sound reflection is achieved through changing the duct cross section, such as in a vehicle exhaust muffler, and sound attenuation is invariably achieved by forcing air through porous media or structures with the exception of some membrane sound absorbers (to be discussed later). Both measures may have detrimental aerodynamic effects, namely high pressure loss, and even causing extra noise called ''self-noise.'' Besides, they are either too bulky or very ineffective in the low-frequency range such as below 500 Hz (Ingard, 1994). To deal with low-frequency noise, there are two types of membrane absorbers whose working mechanisms depend on the strong sound–structure coupling. Ford and McCormick (1969) described an earlier type consisting of layers of thin membranes, such as 0.2-mm aluminum sheets, stacked at a certain distance from one another. They are used in broadcasting studios, concert halls, etc., and substantial sound absorption occurs only at narrow bands around a few resonance frequencies of the membrane-cavity structure. Fuchs and his colleagues developed another type of membrane absorber (Ackermann *et al.*, 1988) in which a perforated thin plate is glued to an all-metal honeycomb structure forming an array of Helmholtz resonators. The device shows two resonance peaks relating to the Helmholtz resonance and the resonance of the cover plate, respectively. Another smooth cover sheet, typically of 0.1-mm-thick aluminum, is then added in front of the perforated plate to protect the resonator from flow and dust. The separation distance is typically 1 mm. The result is an improved performance between the two resonance peaks. Membrane absorbers of this type have provided useful attenuation of low-frequency noise down to some 60 Hz when used in a papermill exhaust (Ackermann and Fuchs, 1989), but exact theoretical prediction proved rather difficult (Frommhold *et al.*, 1994).

Recently, Huang (1999) proposed another type of membrane absorber for low-frequency duct noise. A membrane of moderate length forms part of a duct wall which vibrates in response to grazing incident noise. The membrane experiences flexural waves with phase speed less than the *in vacuo* wave speed, which is in turn much less than the speed of sound in air. It is theoretically demonstrated that (a) substantial reflection of noise is possible without the change in duct cross section area, and (b) the slowly traveling coupled waves provide a powerful mechanism of energy dissipation at an attenuation rate (in dB per unit distance of travel) inversely proportional to the phase speed. Both (a) and, to a lesser extent, (b) are demonstrated experimentally in the present study. Theoretically, the flexural waves can be slowed down indefinitely by increasing the compliance of the membrane, but in practice there is a limit on the membrane thickness that may be used. The present study is motivated by the desire to further understand the coupled waves on a thin membrane under tension. The focus is on the mapping of the whole wave speed spectrum. At low frequencies, the phase speed is found to be less than the *in vacuo* wave speed of the membrane. At higher frequencies, however, waves of speed higher than the speed of sound in air, namely supersonic waves, are also found although not necessarily useful for noise control.

The fact that the speed of waves, including sound waves, is controlled by the compliance of passage walls is well known (Lighthill, 1978). Shallow water waves are the most familiar example where the free surface as a boundary controls the wave speed. Another example is wave propagation in the aorta of large mammals where wave speed ranges from 5 to 10 m/s (Lighthill 1978, p. 99). In the broader context of biological applications, Shapiro (1977) studied the incompressible flow through flexible tubes where the very low eigenwave speed replaces the usual sound speed in controlling the flow behavior, some of which is quite extraordinary. For example, when the flow speed exceeds the eigenwave speed, friction causes static pressure to rise instead of falling, similar to supersonic airflow in the contraction–expansion nozzle. Physical experiments using water have also been constructed to demonstrate such an effect (Kececioglu *et al.*, 1981). In the area of wave attenuation, Horne and Hansen (1982) demonstrated that as much as 60-dB reduction could be achieved by the coupling of water wave and the pipe wall of comparable acoustic impedance. In a separate work by Dunlop (1992), the speed of sound in such a coupled system was measured and the result was shown to agree with simple theory. A more general coverage of this topic was recently given by Fahy (1997).

Similar examples do not seem to exist in airflow through collapsible tubes in the sense that most such experiments were conducted in a starling-resistor-type configuration (e.g., Gavriely *et al.*, 1989). In such cases the tube collapses in one cross section, this can hardly be modeled as a long channel of uniform property. On the other hand, some theoretical attempts have been made in the context of submerged structure (Ko, 1994) to resolve the eigenvalues of structural vibrations coupled with either air or water flow inside a duct. The duct considered in the example is made of 2-in.-thick steel. The structure-to-fluid mass ratio is very high when the fluid is air, and is of the order of unity when the fluid is water. In both cases subsonic eigenwaves are found. Whether the eigenvalues found in the case of very high mass ratio represent anything significant in reality has not been validated experimentally. Supersonic eigenwaves are inadmissible in Ko's model because of the presence of external fluid which extends to infinity. The present study aims to explore the coupled waves in a laboratory experiment using a tensioned membrane whose mass ratio is of the order of unity and the external fluid is limited to a finite cavity. Acoustic excitation is used and the sound waves measured over the membrane shows dominating features of the eigenvalues found theoretically. As a first attempt to understand the physics the effect of flow has not been included. The possibility of flow-induced vibration is also postponed, but it is believed that a clear understanding of wave behavior without flow could benefit such instability studies in the future.

In what follows, the eigenwave speed in a duct of infinite length is first calculated, the main results being the prediction of both subsonic and supersonic phase speeds in air depending on frequency. The existence and significance of these wave speeds are then examined experimentally in a duct with finite length. Both subsonic and supersonic waves are found.

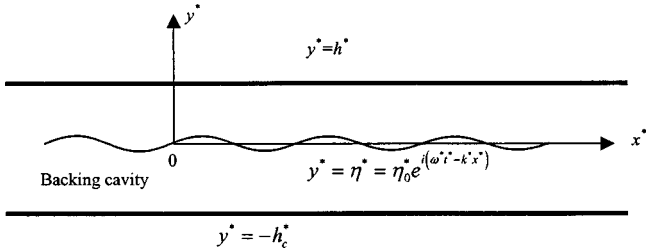

FIG. 1. Geometrical configuration of the theory.

I. THEORY

To illustrate the acoustic principle, a simple configuration of two-dimensional channel of height h^* with a single lower flexible wall at $y^*=0$ is considered, as shown in Fig. 1. The word ''duct'' will still be used in the text, but the three-dimensional effect is not considered theoretically. Some three-dimensional effects are inevitable in the experiment, but the agreement between the measured data and the two-dimensional prediction is satisfactory after taking special precautions to minimize these effects. It is assumed that the flexible wall is very thin and the only mechanical restoring force against displacement is the tensile stress applied. The flexible wall vibrates and radiates sound externally, and the so-called breakout noise will be important (Cummings, 1994) in the context of ventilation noise. In order to avoid such leaking, and more importantly to avoid the three-dimensional effect in the experiment, we consider an additional lower rigid wall at $y^*=-h_c h^*$, where h_c is the ratio of channel heights. The flexible wall has a mass per unit area of M^*, a damping coefficient D^*, and a tensile force T^* is applied. The flexible wall is subject to a traveling wave perturbation of displacement

$$\eta^* = \eta_0^* e^{i(\omega^* t^* - k^* x^*)}.$$

Under these conditions, what is the characteristic flexural wave speed $c^*=\omega^*/k^*$? Note that, in an infinite duct, there cannot be separate wave speeds for the structural and air motions although the same may not be true in the experiment where the structure is finite. A similar model excluding the effect of external fluid was briefly studied in a previous paper (Huang, 1999). The result of that model will now be used as a special case for comparison.

All variables are normalized by three basic quantities ρ_0^*, h^*, and c_0^*. Here ρ_0^* and c_0^* are, respectively, the air density and isentropic speed of sound in free space. After normalization these variables are denoted by

$$\begin{aligned}
&x=\frac{x^*}{h^*}, \quad y=\frac{y^*}{h^*}, \quad t=\frac{c_0^* t^*}{h^*}, \quad \eta_0=\frac{\eta_0^*}{h^*},\\
&c=\frac{c^*}{c_0^*}, \quad \omega=\frac{\omega^* h^*}{c_0^*}=k_0, \quad k=\frac{\omega}{c},\\
&M=\frac{M^*}{\rho_0^* h^*}, \quad c_T=\frac{\sqrt{T^*/M^*}}{c_0^*}, \quad D=\frac{D^*}{\rho_0^* c_0^*},\\
&\phi=\frac{\phi^*}{c_0^* h^*}, \quad p=\frac{p^*}{\rho_0^* (c_0^*)^2},
\end{aligned} \tag{1}$$

where M, D, and c_T are, respectively, the mass ratio, the dimensionless damping coefficient, and the *in vacuo* panel wave speed, and ϕ and p are, respectively, the dimensionless perturbation velocity potential and sound pressure inside the channel. Note that the dimensionless angular frequency ω is equal to the dimensionless wave number based on c_0^* and k_0, and is related to the ratio of the driving frequency, f^*, to the first cut-on frequency of sound in the rigid channel, f_1^*, by a factor of π. Thus

$$\omega = k_0 = \pi f, \quad \text{where } f = f^*/f_1^* \quad \text{and } f_1^* = c_0^*/2h^*.$$

In dimensionless form, the wave equation in fluid becomes

$$\left(-\frac{\partial^2}{\partial t^2} + \nabla^2 \right) \phi = 0,$$

which, for harmonic excitation, is reduced to the Helmholtz equation

$$\frac{\partial^2 \phi}{\partial y^2} = k_a^2 \phi,$$

where, for real wave number k,

$$k_a^2 = k^2 - k_0^2, \quad k_a = \begin{cases} \sqrt{k^2 - k_0^2}, & c < 1, \ k > k_0, \\ i\sqrt{|k^2 - k_0^2|}, & c > 1, \ k < k_0. \end{cases} \tag{2}$$

Here k_a is real for subsonic waves but imaginary for supersonic waves. The solution for the perturbation velocity potential inside the channel satisfying the following rigid wall condition and the kinematic condition on the flexible wall,

$$\left.\frac{\partial \phi}{\partial y}\right|_{y=1} = 0, \quad \left.\frac{\partial \phi}{\partial y}\right|_{y=0} = \frac{\partial \eta}{\partial t} = i\omega\eta,$$

is

$$\phi = -\frac{i\omega\eta}{k_a} \frac{e^{k_a(1-y)} + e^{-k_a(1-y)}}{e^{k_a} - e^{-k_a}}. \tag{3}$$

The pressure perturbation on the upper side of the flexible wall, $y = 0+$, is denoted by p_+,

$$p_+ = -\left.\frac{\partial \phi}{\partial t}\right|_{y=\eta} = -\frac{\omega^2 \eta}{k_a} \coth k_a. \tag{4}$$

The boundary conditions for the perturbation velocity potential in the lower channel are

$$\left.\frac{\partial \phi}{\partial y}\right|_{y=-h_c} = 0, \quad \left.\frac{\partial \phi}{\partial y}\right|_{y=0} = \frac{\partial \eta}{\partial t} = i\omega\eta,$$

so that

$$\phi = +\frac{i\omega\eta}{k_a} \frac{e^{k_a(h_c+y)} + e^{-k_a(h_c+y)}}{e^{k_a h_c} - e^{-k_a h_c}}.$$

Similarly, the pressure on the lower surface is found to be

$$p_- = -\left.\frac{\partial \phi}{\partial t}\right|_{y=0} = +\frac{\omega^2 \eta}{k_a} \coth k_a h_c. \tag{5}$$

The wave impedance of the fluid loading on the wall is defined and calculated as follows:

$$Z = \frac{p_+^* - p_-^*}{\rho_0^* c_0^* d\eta^*/dt^*} = \frac{p_+ - p_-}{i\omega\eta} = \begin{cases} +i\dfrac{k_0}{k_a}[\coth k_a + \coth k_a h_c], & \text{for } c < 1; \\ -i\dfrac{k_0}{|k_a|}[\cot(|k_a|) + \cot(|k_a h_c|)], & \text{for } c > 1. \end{cases}$$

For long waves without change of amplitude, $|k_a| \ll 1$, hence $\coth k_a$ and $\cot(|k_a|)$ are positive. The effect of fluid loading on the wall dynamics is the added mass for subsonic waves; however, for supersonic waves it is a spring stiffness. The presence of a trigonometric function in the supersonic case signifies oblique wave fronts similar to those in the high-order duct modes with rigid boundaries. The dynamics of the flexible wall is described by the equation

$$T\frac{\partial^2 \eta}{\partial x^2} - D\frac{\partial \eta}{\partial t} + p_- - p_+ = M\frac{\partial^2 \eta}{\partial t^2}, \tag{6}$$

where the damping coefficient D may be substituted by $M\omega\sigma$ after invoking the concept of complex Young's modulus. Here, σ is the loss factor of the material defined as the ratio of energy lost per radian to the maximum potential energy. Inserting the fluid pressures of Eqs. (4) and (5), Eq. (6) becomes

$$M\omega^2(1 - i\sigma) + \frac{\omega^2}{k_a}[\coth k_a + \coth k_a h_c] - Mc_T^2 k^2 = 0. \tag{7}$$

Mathematically, the complex eigenvalue $k = k_r + ik_i$ has to be sought on the entire complex plane. But in reality, only those in the fourth quadrant of the complex plane, $k_r > 0$, $k_i < 0$, are of physical interest. These eigenvalues represent propagating waves with decaying amplitude. For a lossless material, $\sigma = 0$, numerical search in this wave number quadrant indicates that eigenvalues exist only on the pure real axis, $k = k_r$, and on the pure imaginary axis, $k = ik_i$. The former represents free waves propagating in the axial direction, while the latter represents standing waves between the hard wall and the flexible wall, which we call the vertical mode. In both cases there is no amplitude decay in the direction of wave travel. This is understandable since there is no energy dissipation mechanism when $\sigma = 0$. When there is damping ($\sigma > 0$), however, the eigenvalues are expected to be complex. The numerical results show that there is no sudden jump in solutions when the damping approaches zero. The following numerical procedure is used to find the complex eigenwave number which then gives the eigenwave speed $c = \omega/k_r$ and the attenuation in decibels per unit distance of h^*,

$$\alpha = 20\log_{10} e^{-k_i} = -8.686 k_i.$$

Given the flexible wall parameters M, c_T, and σ, the lower channel height h_c, and angular frequency ω, c and k_i are the two independent variables in Eq. (7). The value of the left-hand side of Eq. (7), denoted as z, is calculated over a uni-

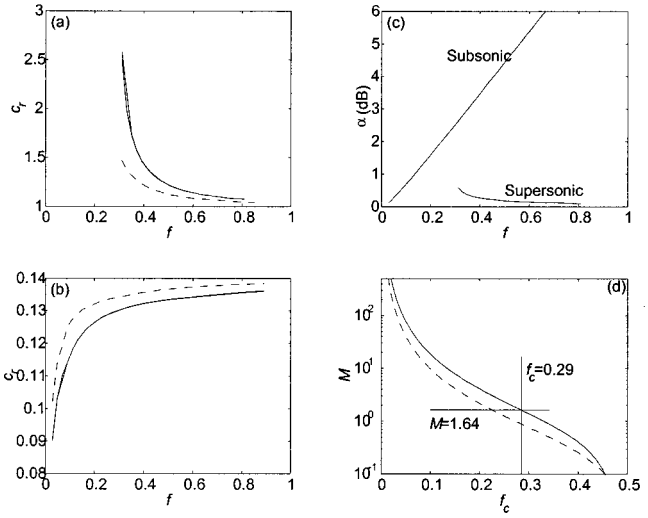

FIG. 2. Theory of sound propagation in a channel with a flexible wall with $M=1.64$ and $c_T=0.14$. Three cases are calculated: (I) lossless flexible wall without external fluid loading for which the results are shown in dashed lines; (II) lossless flexible wall with a lower channel of depth ratio $h_c=1.1$; and (III) flexible wall of loss factor $\sigma=0.1$ with lower channel of $h_c=1.1$. Note that cases II and III are shown in solid lines but the differences are too small to distinguish. (a) is the supersonic eigenwave speed. (b) is the subsonic eigenwave speed. (c) is the attenuation rate for case III. (d) is the functional relationship between mass ratio and the ''cut-on'' frequency for supersonic eigenwaves.

form mesh on the plane of c and k_i. The eigenvalues of c and k_i are found by the intersections of contour lines of $\mathrm{Re}(z)=0$ and $\mathrm{Im}(z)=0$ utilizing Matlab software.

Figure 2 is an example which covers the parameters used in the experiments: $M=1.64$ and $c_T=0.14$. Three cases are calculated; case I is a lossless wall without external fluid loading, namely with external vacuum, and is shown in the figures as dashed lines; case II is the lossless wall with a lower rigid wall forming a second channel of width $h_c=1.1$; case III is based on case II, but with a loss factor $\sigma=0.1$ which is of the order of magnitude expected of the membrane material used in the experiments. Figure 2(a) and (b) is the eigenwave speeds for the three cases mentioned. The two solid lines are for cases II and III, respectively, but they can hardly be distinguished from one another. This means that for the normal materials the eigenwave speed is hardly influenced by its friction. Figure 2(b) shows that subsonic eigenwaves approach $c_T=0.14$ as $f\to\infty$, which can be demonstrated as follows. As $k_a\to k_0\to\infty$, $\coth k_a/k_a$ and $\coth k_a h_c/k_a\to 0$. Equation (7) then gives $c\to c_T$ for the simple case of $\sigma=0$. Figure 2(b) shows the supersonic eigenwaves which are only found for frequencies above a certain value to be explained with Fig. 2(d).

Figure 2(c) gives the sound attenuation rate α (in dB per distance equal to the channel height h^*) for both subsonic and supersonic eigenwaves. Supersonic waves hardly decay, but subsonic waves experience attenuation compatible with that of sound propagating through a duct lined with porous sound absorption materials (Ingard, 1994). The reason for such a high attenuation in the present case is that the wave speed is much lower so that, for a unit travel distance, the resident time is longer and the frictional losses are greater.

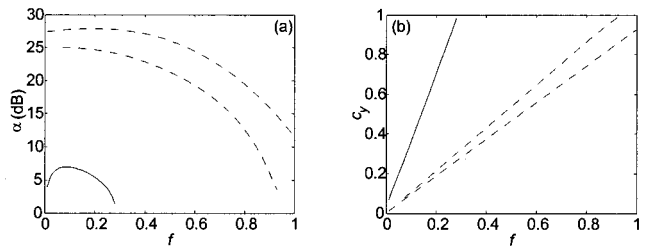

FIG. 3. Vertical mode for lossless membrane with $M=1.64$, $c_T=0.14$, and $h_c=1.1$. (a) is the axial attenuation rate and (b) is the vertical wave speed. The solid curve in (a) corresponds to the solid curve in (b), and similarly for the dashed curves, in the same clockwise order.

The attenuation is also proportional to frequency which is inherited from the simple damping model adopted, $D=M\omega\sigma$. Thus, at intermediate and high frequencies, say $f>0.3$, it would be impossible to observe these waves, although theoretically they are found to coexist with supersonic waves. This is consistent with our experimental observation that subsonic waves can hardly be measured beyond 500 Hz.

The frequency of the wave speed singularity ($c_r\to\infty$) shown in Fig. 2(a) may be called the critical frequency, f_c, above which supersonic waves may occur, namely supersonic cut-on frequency. f_c may be found by letting $k=\omega/c\to 0$, $k_a\to ik_{0c}$, and $k_{0c}=\pi f_c$, so that for $\sigma=0$ Eq. (7) immediately gives the following relationship:

$$M=[\cot k_{0c}+\cot k_{0c}h_c]/k_{0c}, \tag{8}$$

which is shown in Fig. 2(d). Here f_c reduces as M increases, and in this particular example $f_c=0.29$. The comparison between cases I and II in the figure means that the lower channel, or air cavity, adds virtual mass to the membrane. Note that $\cot k_{0c}$ and $\cot k_{0c}h_c$ are periodic functions of k_{0c}. That means for a single mass ratio M, there are multiple critical frequencies associated with the multiple solutions for k_{0c}. In the example given above, the range of frequency is restricted to the first cut-on of the duct and the backing cavity, $k_0<\pi$, $k_0h_c<\pi$. As a result, there is only one critical frequency k_{0c} found. In the experiment, this means a frequency ceiling of 5 kHz for a square duct of 3 cm in cross section.

The vertical mode mentioned earlier for a lossless membrane, $\sigma=0$, has a pure imaginary eigenwave number $k=ik_i$. In this case, $k_a=ik_{ai}$ where $k_{ai}=\sqrt{k_i^2+k_0^2}$, and $k_a^{-1}\coth k_a=-k_{ai}^{-1}\cot k_{ai}$. The vertical wave speed is $c_y=\omega/k_{ai}$. The result is shown in Fig. 3 for a configuration identical to that of Fig. 2. The range for the search is limited to $-k_i<3.5$. Two modes are found in this range. One is the slowly decaying mode (solid curves) which meets the no-decay limit of $\alpha=0$ at the critical frequency predicted earlier, $f_c=0.29$, and the other (dashed curves) has a rather high attenuation rate in the axial direction. Note that the vertical wave speed reaches unity, $c_y=1$, at the critical frequency for the less damped mode. The possible presence of this mode in a duct of finite length could confuse the axially propagating modes near the edges of the membrane, but the problem is expected to diminish after a distance equal to a few duct height h^*.

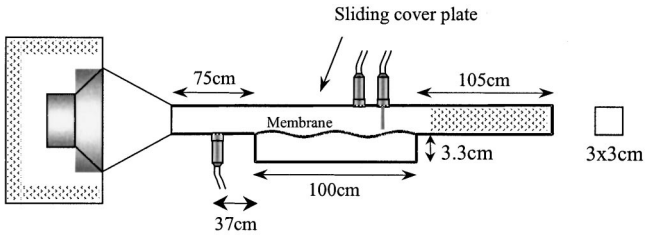

FIG. 4. The setup of the rig.

Mathematically speaking, the plane wave mode, $k=k_0$, is always a possible solution when the backing cavity is present. This solution is seen when the membrane experiences no displacement, $\eta=0$, and the two sides of the membrane experience equal pressure disturbance, $p_+=p_-$. This mode is mathematically trivial for the configuration of infinite duct, but it may become physically significant when the duct is finite. This is observed in the following experiment.

II. EXPERIMENTAL SETUP AND DATA PROCESSING

The rig is shown in Fig. 4. A loudspeaker driver unit of 6-in. diameter with 40-Hz resonance frequency is enclosed in a wooden box and is driven by a function generator and amplifier. The duct has a square cross section of 3×3 cm^2 and is coupled with the loudspeaker via a contraction cone. The duct has three regions: an upstream part of 75-cm length with rigid walls, a test section with a 1-m-long membrane on the lower side, and a downstream section with a 15-cm-long rigid wall and a 90-cm-long section filled with sound absorption material. Complete sound absorption is not expected since reflection occurs at the leading and trailing edges of the membrane anyway. The membrane is backed by a lower cavity 3.3 cm in depth to prevent breakout noise. A tensile force of 4.0 N, which produces 10% membrane elongation, is applied. The membrane used is 3M's transparent dispenser tape of thickness 0.065 mm and mass per unit area of $M^*=60\,\mathrm{g/m^2}$. In order to best model a two-dimensional configuration, a small clearance of less than 0.5 mm is allowed between the tensioned membrane and the side walls of the duct. Tests with the small gap sealed were also carried out (see later). Sound traveling over the membrane is expected to have a phase speed different from the normal speed of sound of about 340 m/s at a room temperature of 15 °C. The dispersion relation $c(f)$ is the main objective of the measurement.

Two B&K $\frac{1}{4}$-in. condenser-type microphones (type number 4135 with ±1-dB amplitude response from 6 Hz to 14 kHz) are installed flush with the duct walls: one at 37 cm upstream of the membrane and the other on the rigid wall opposite the membrane, which is designed to slide back and forth so that all axial locations can be covered with just a few microphone insertion holes. To get the sound field of the whole length over the membrane at repeatable loudspeaker excitation, the signal taken from the ''mobile'' microphone over the membrane section is compared with that from the upstream microphone which acts as a reference. The amplitude ratio and phase difference between the two pressure measurements are determined using the data acquisition and analysis system described below. A probe microphone (B&K type 4182) with a 5-cm stiff probe head of 1.24-mm diameter is inserted through the sliding plate next to the $\frac{1}{4}$-in. microphone. It moves along with the $\frac{1}{4}$-in. microphone and is used to measure the sound pressure right above the membrane surface. The frequency response of this probe is 3 dB down from dc to 2 kHz which is the maximum frequency required for the probe measurement. The probe microphone measurement is necessary because the sound amplitude decays exponentially in the y direction for subsonic waves and the ratio of pressure measured by the two microphones at the same axial coordinate can be estimated from Eq. (3), or

$$\frac{p|_{y=0}}{p|_{y=1}}=\frac{\phi|_{y=0}}{\phi|_{y=1}}=\frac{e^{k_a}+e^{-k_a}}{2}=\cosh k_a\,.$$

For example, according to the solid line shown in Fig. 2(b), at $f=0.2$, $c_r=0.1265$, $k_a=4.9278$, and $\cosh k_a=69.0$. Experimental data indeed shows that subsonic waves are more evident near the membrane surface than on the opposite wall.

The microphones are supported by the B&K's Nexus four-channel conditioning amplifier (type 2693) and the signals are fed into a Pentium 266MHz DELL PC installed with a National Instruments AD card (type PCI-MIO-16-E-1) controlled by the LabVIEW software. Three narrow-band frequency sweeps (or chirps) are generated from the function generator: 50–300 Hz, 300 Hz to 2.5 kHz, 2.5–5 kHz. The sweep is linear ''ramp-up'' and the durations are 4, 2, and 1 s, respectively. The AD card sampling frequencies are 4, 16, and 32 kHz for the three bands, respectively, and data sampling is carried out over one sweep cycle. The three-band separation is necessary because the conditioning amplifier for the microphone requires a different setting in order to maximize the true resolution of the A/D conversion. The spatial step for the ''sliding'' microphones is 2 cm for low frequencies and 1 cm for high frequencies. This step size is found to be sufficiently small to resolve the waveforms. For each position, the amplitude ratio and phase angle relative to the reference microphone are found at all frequencies. The data output is then sorted out in terms of amplitude and phase distribution along the membrane for all individual frequencies. A set of harmonic excitation tests were also carried out, which confirmed the validity of the chirp measurement.

Taking $\rho_0^*=1.225\,\mathrm{kg/m^3}$ and $c_0^*=340\,\mathrm{m/s}$, the dimensionless parameters M and c_T are calculated as follows,

$$M=\frac{60\times10^{-3}}{1.225\times0.03}=1.64,$$

$$c_T^*=\sqrt{\frac{4.0\ \mathrm{N}}{0.0603\ \mathrm{kg/m}\times0.03\ \mathrm{m}}}=47.0\ \mathrm{m/s},$$

$$c_T=\frac{c_T^*}{c_0^*}=0.14,$$

for which the supersonic cut-on frequency is predicted at

$$f_c=0.2854,\quad f_c^*=1617\ \mathrm{Hz}.$$

The real damping for the membrane is also a function of the applied tension and the measurement of such a parameter requires vacuum environment which is not available in the

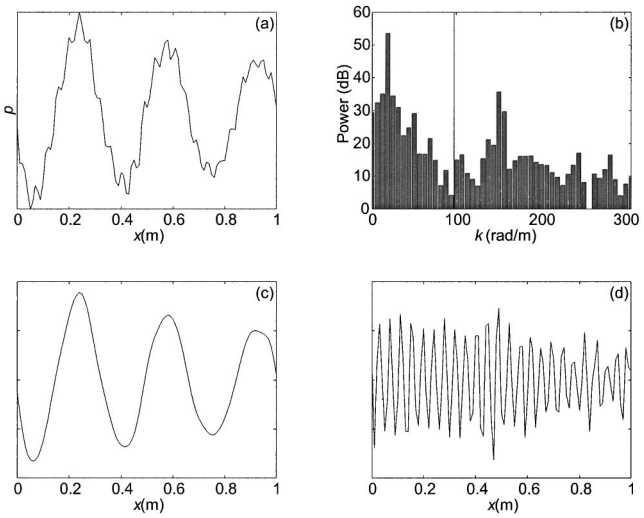

FIG. 5. Analysis of spatial sound pressure distribution for frequency 1030 Hz. (a) is the pressure waveform and (b) is the spectrum in which two peaks are identified within the two bands which are used to construct bandpass signals shown in (c) and (d). The speed of sound represented by the two peaks are 344.0 and 42.7 m/s, respectively.

present study. As a result the analysis on the damping of sound waves is only qualitative.

The amplitude and the phase angle of the pressure signals taken by the mobile microphone are compared with the simultaneous measurement taken by the upstream reference microphone. The amplitude ratio and the phase delay are found and used to construct the pressure distribution along the membrane. This distribution is equivalent to the simultaneous measurement for all points. Shown in Fig. 5 is an example taken at 1030 Hz. Figure 5(a) is the measured axial pressure distribution which shows long waves being modulated by short waves. Since the membrane length is limited, the number of wave cycles found is few and the wave number resolution is therefore limited to 1 m^{-1}. In most cases the true wave number may fall between two discrete wave numbers given by the discrete Fourier transform and the spectral leaking is corrected by taking the spectral center-of-gravity, $k_{\text{peak}}=\Sigma k_j P_j/\Sigma P_j$, where P and k are spectral power and wave number, respectively, over five wave number points, two on the left and two on the right of the apparent spectral peak. Wave speed c_r is then found by ω/k_{peak}. With this procedure two peaks can be identified in the power spectrum shown in Fig. 5(b), one at $k=18.8$ rad/m and the other at $k=151.6$ rad/m, corresponding to wave speeds of $c=344.0$ and 42.7 m/s, respectively. In order to see the spatial features of the two perceived wave components, the spectrum is divided into two parts shown by the thin solid line in Fig. 5(b). Inverse FFT is applied to each side and the decomposed waveforms are shown in Figs. 5(c) and 5(d), the latter being amplified for easier observation. The long wave propagates at sonic speed and the short wave has phase speed close to $c_T^*=47.0$ m/s. In this case the sonic wave dominates and both waves show apparent spatial decay. But the exact attenuation rate cannot be calculated directly from the amplitude envelope due to the presence of significant wave reflection. The spectral decomposition is similar to the harmonic wavelet transform found by Newland (1993), who chose to utilize the octave bands as the convenient segmentation and showed that a set of orthogonal harmonic wavelets may be defined as

$$\omega(x)=(e^{i4\pi x}-e^{i2\pi x})/i2\pi x$$

for dimensionless wave number from 2π to 4π. The magnitude of such a wavelet decays as $(2\pi x)^{-1}$, which is much less compact than other popular wavelet techniques. However, the latter suffer from the fact that a clear physical interpretation for the wavelets is not always possible. Therefore, the concept of harmonic wavelet is chosen with flexible choice of spectral bands adopted. The wider the spectral band, the more compact the wavelet becomes and the better the spatial resolution it gives. In the present case, only two bands are chosen in order to maximize the spatial resolution.

Note that an impulse-style measurement is not appropriate in this study because (a) reflections occur very close to the test sections, leaving no time window for low-frequency measurement, and (b) excitation of higher duct modes may seriously pollute the data at moderate to high frequencies.

III. RESULTS AND DISCUSSION

Before analyzing the experimental data, it has to be borne in mind that the theoretical predictions shown in Fig. 2 were made for a duct of infinite length. Thus, the sound radiated by the flexural waves definitely manifest themselves into traveling waves of a single phase speed. In a finite duct, however, such sound waves could interact with the scattering at the leading and trailing edges of the membrane to produce a complicated pattern. Nevertheless, the acoustic field can be tactically divided into two parts: one part is the normal standing wave pattern in a finite duct of partially reflecting ending if the membrane were replaced by a rigid wall, while the other part is the wave radiated by the membrane vibration which is itself induced by the incident sound. The present interest lies in the latter, namely, the second peak shown in Fig. 5(b), which may or may not dominate the spectrum.

Two factors need to be clarified before analyzing the results. One is the influence of the backing cavity, and the other is the edge scattering. As shown in Fig. 4, the lower rigid wall is added to prevent breakout noise. But more importantly, the backing cavity enables the rig to simulate wave propagation in two spatial dimensions for which a theory is easily constructed for comparison. It is likely that the very light and limp membrane partition is almost transparent to sound waves. A plane wave mode propagating at the normal speed of sound of 340 m/s may dominate in some frequency ranges. For this mode, the membrane does not experience any vibration and the result is a trivial solution for the membrane dynamics. This outcome does not necessarily imply weak or no coupling between the sound and the membrane for other configurations. The second factor addressed here is the effect of scattering by the two edges of the membranes. All physically admissible eigenmodes may be excited and our attention is focused on whether the propagating mode dominates. Vertical modes shown in Fig. 3 have moderate to high attenuation rates, and are therefore unlikely to dominate

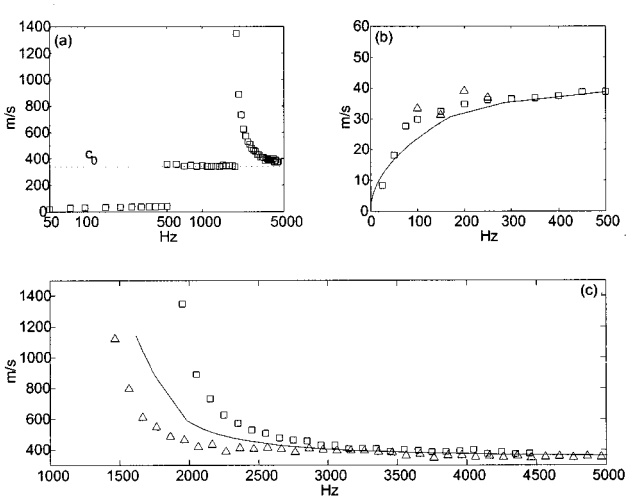

FIG. 6. Comparison of the dispersion relationship between theory and experiments. (a) is the overall distribution of experimental data, and (b) is the zoom-in view of the data in the subsonic regime. Theoretical prediction is given by the solid curve, squares are from the probe microphone measurement on the membrane surface, and triangles are from the $\frac{1}{4}$-in. microphone measurement of pressure on the hard wall. (c) compares the measured supersonic wave speeds with theoretical predictions (solid line). The squares are for the membrane with small sideway gaps simulating two-dimensional wave field and triangles are data taken when the gap is covered.

the waveforms over the bulk length of the membrane except for frequencies very close to the supersonic cut-on.

Including only the dominant propagating waves, Fig. 6(a) gives the dispersion relationship deduced from one set of experimental data using the sliding $\frac{1}{4}$ in. microphone flush with the rigid wall. The sound waves propagating at the normal speed of sound are always present, and are in fact dominant below 500 Hz. The reason why the normal speed of sound is not shown in the figure is that the test section is too short to have a complete waveform below 500 Hz. In spectral analysis, one finds that the corresponding spectral peak is located at $k \rightarrow 0$ as shown later in Fig. 7. Beyond 500 Hz, waves with $c_0 = 340$ m/s can be resolved and seen as an isolated peak in the wave number spectrum. The accompanying subsonic waves is rather weak, as shown in Fig. 5 for the probe microphone measurement near the membrane surface, and are not shown in Fig. 6(a) beyond 500 Hz. Note that 500 Hz happens to be where the spectral dominance changes from the subsonic wave number to the sonic wave number. It does not represent a cutoff frequency for the subsonic waves.

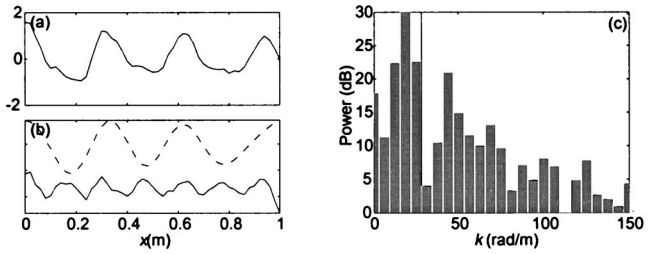

FIG. 7. Typical subsonic waveform found at frequency 250 Hz. (a) is the real part of the complex waveform measured by the probe microphone. (b) shows the wavelets representing the sonic wave (upper) and subsonic wave (lower) of speed 46 m/s. (c) is the spectrum showing the decomposition boundary.

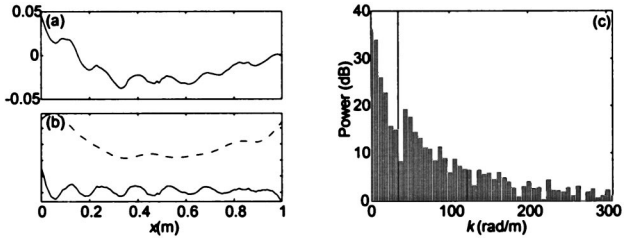

FIG. 8. Typical supersonic wave measured at frequency 2200 Hz. (a) is the measured pressure distribution, and (b) is the decomposed wavelets based on the spectral division shown in (c). The dashed line in (b) has speed 731 m/s.

Supersonic waves are found to be dominant beyond about 2 kHz, but, in this case, the frequency does represent the cut-on for the supersonic waves, although not a cutoff for the sonic waves either.

Figure 6(b) compares the prediction of subsonic waves with the experimental data. The quantitative agreement between theory and experiment is satisfactory. Note that subsonic waves can only be detected up to 250 Hz for the pressure on the rigid wall (data points indicated by △). This is consistent with earlier theoretical observation that pressure oscillation decays exponentially across the channel.

Figure 6(c) compares the theory with experimental data beyond the critical frequency. The predicted critical frequency is $f_c = 1617$ Hz. The data shows a maximum of 1348 m/s at 1950 Hz for the membrane with a side-gap allowance (□). In general, there is good agreement between theory and data, but the critical frequency is predicted under by about 333 Hz. It is suspected that this discrepancy could be caused by the gap between the membrane and the side walls. This conjuncture was tested by sealing up the gap with minimal extra membrane material without tensile force. The results are presented as the triangular (△) points. The maximum wave speed is 1120 m/s and it occurs at a frequency of 1465 Hz, which is 152 Hz lower than f_c predicted by the two-dimensional theory. Such results may be understood from the point of view of effective mass of the membrane vibration. When there is a gap, the pressure difference between the upper and lower surfaces of the membrane vanishes around the edges. As a result, the edges do not vibrate as much as elsewhere and the membrane as a whole appears lighter. This leads to a smaller equivalent M and a higher f_c (see Fig. 2). When the gap is sealed, the pressure difference across the width may be very uniform, but the restraint at the membrane edges makes the structure effectively heavier than it really is. Note that the maximum speed of sound that can be obtained with confidence in the signal processing is limited by the membrane length. For example, at the observed top wave speed in Fig. 6(c), the wavelength is nearly 0.7 m. However, wave speeds higher than 2000 m/s were deduced from the constant phase angle slope of a single traveling wave observed when the lower rigid wall was removed, but meaningful analysis of such configuration can only be carried out with a three-dimensional theory for the breakout waves.

Typical subsonic and supersonic waveforms are given in Figs. 7 and 8 using the method described earlier in Fig. 5.

The spectra are divided into two blocks and the decomposed ''wavelets'' correspond to sonic waves and those radiated by the membrane response. These examples differ from the earlier ones in that the sonic waves do not dominate the overall waveform. The spectral division for the two waves is not as clear-cut as in Fig. 5 since the two wave numbers are closer together and the wave number resolution is limited by the total length of the membrane section. Figure 7 shows that at 250 Hz, subsonic waves undulate the long wave, which is mainly made up of sonic waves plus the effects of scattering by the edges. The subsonic wave speed is found to be 46 m/s and the amplitude clearly decays downstream. However, the attenuation rate is not analyzed due to the difficulties of (a) the measurement of damping coefficient for the thin membrane under tension, and (b) the calculation of exponential decay rate at the presence of edge scattering and significant wave reflection. A typical supersonic wave is illustrated in Fig. 8 in which the long wave, the dashed line in Fig. 8(b), has a wave speed of 731 m/s.

The prevailing sound speed over the membrane section is also evident from the measurement of the ratio of sound amplitude to the reference point, which is located 37 cm upstream of the membrane. The wave amplitudes at the membrane leading edge are 0.08 and 1.64, respectively (both calibrated by the microphone responses), for the two examples. For the subsonic case, sound with a low amplitude is a clear indication that the interface (membrane leading edge) is nearly a pressure node like the open end of a duct, consistent with the expectation that the effect of the membrane may be similar to filling the duct with a gas medium with a low sound speed. For the supersonic case, the amplitude ratio is greater than unity and is indicative of solid-wall-style sound reflection. Such reflection could not have been caused by the boundary far downstream since the absorption ending works sufficiently well for frequencies above 2 kHz.

In the intermediate frequency range from 500 Hz to the supersonic cut-on frequency, the prevailing sound speed is the normal value of 340 m/s, which was earlier described as a ''trivial'' solution for the membrane dynamics. This is consistent with the theoretical observation of fast spatial decaying rate experienced by the subsonic waves on the membrane, cf. Fig. 2(c).

IV. CONCLUSIONS

Experimental studies have been carried out to demonstrate the strong coupling between sound and structure when the structure-to-fluid mass ratio is of the order of unity. A 1-m-long thin membrane under tension was used in the experiment and the data shows a close agreement with eigenvalue predictions for wave propagation in an infinite duct with flexible walls. Sound speeds as low as 8.3 m/s and as high as 1350 m/s have been measured. The departure from the normal value of 340 m/s over the membrane section results in a significant amount of wave reflection at the interface of the rigid and flexible sections of the duct. The speed of eigenwave over the membrane may be understood from the viewpoint of the mass-spring system of the fluid-loaded membrane. At low frequencies, the effect of fluid is purely masslike and the result is a membrane heavier than its own weight. The wave speed is slower than the *in vacuo* value, which, in this example is determined by the tensile force applied. At higher frequencies the effect of fluid loading is springlike and the eigenwave is found to be faster than the speed of sound in free space. At a particular frequency the effect of mass and spring balance each other, and singular sound speed is predicted for a lossless system. The frequency at which this singularity occurs depends only on the mass ratio and close agreement with experimental data is obtained. At supersonic speed, waves travel in a way similar to the high-order modes in a rigid duct where the sound waves advance in a zig-zag path with supersonic axial wave speed.

ACKNOWLEDGMENTS

The authors thank Professor F. P. Mechel for his many useful comments on the original paper. The work is part of a project (Grant No. G-S583) funded by The Hong Kong Polytechnic University which also supports the research studentships of Y.S.C. and T.L.C.

Ackermann, U., and Fuchs, H. V. (**1989**). ''Noise reduction in an exhaust stack of a papermill,'' Noise Control Eng. J. **33**(2), 57–60.

Ackermann, U., Fuchs, H. V., and Rambausek, N. (**1988**). ''Sound absorbers of a novel membrane construction,'' Appl. Acoust. **25**, 197–215.

Beranek, L. L., and Ver, I. L. (eds.) (**1992**). *Noise and Vibration Control Engineering* (Wiley, New York).

Cummings, A. (**1994**). ''Attenuation of sound in unlined ducts with flexible walls,'' J. Sound Vib. **174**, 433–450.

Dunlop, J. I. (**1992**). ''Measurement of acoustic attenuation in marine sediments by impedance tube,'' J. Acoust. Soc. Am. **91**, 460–469.

Fahy, F. J. (**1997**). ''Acoustic interaction between structures and fluids,'' in *Encyclopedia of Acoustics*, edited by Malcolm J. Crocker (Wiley, New York), Vol. 1, Chap. 10.

Ford, R. D., and McCormick, M. A. (**1969**). ''Panel sound absorbers,'' J. Sound Vib. **10**, 411–423.

Frommhold, W., Fuchs, H. V., and Sheng, S. (**1994**). ''Acoustic performance of membrane absorbers,'' J. Sound Vib. **170**(5), 621–636.

Gavriely, N., Shee, T. R., Cugell, D. W., and Grotberg, J. B. (**1989**). ''Flutter in flow-limited collapsible tubes: a mechanism for generation of wheezes,'' J. Appl. Phys. **66**, 2251–2261.

Horne, M. P., and Hansen, R. J. (**1982**). ''Sound propagation in a pipe containing a liquid of comparable acoustic impedance,'' J. Acoust. Soc. Am. **71**, 1400–1405.

Huang, L. (**1999**). ''A theoretical study of duct noise control by flexible panels,'' J. Acoust. Soc. Am. **106**, 1801–1809.

Ingard, K. U. (**1994**). *Notes on Sound Absorption Technology* (Noise Control Foundation, New York).

Kececioglu, I., McClurken, M. E., Kamm, R. D., and Shapiro, A. H. (**1981**). ''Steady, supercritical flow in collapsible tubes. Part 1. Experimental observations,'' J. Fluid Mech. **109**, 367–389.

Ko, S. H. (**1994**). ''Sound wave propagation in a two-dimensional flexible duct in the presence of an inviscid flow,'' J. Sound Vib. **175**, 279–287.

Lighthill, M. J. (**1978**). *Waves in Fluids* (Cambridge U.P., Cambridge).

Newland, D. E. (**1993**). ''Harmonic wavelet analysis,'' Proc. R. Soc. London, Ser. A **443**, 203–225.

Shapiro, A. H. (**1977**). ''Steady flow in collapsible tubes,'' Trans. ASME J. Biomech. Eng. **99**, 126–147.